

**The following resources related to this article are available online at [www.sciencemag.org](http://www.sciencemag.org) (this information is current as of November 13, 2009 ):**

**Updated information and services**, including high-resolution figures, can be found in the online version of this article at:

<http://www.sciencemag.org/cgi/content/full/326/5955/962>

This article **cites 6 articles**, 3 of which can be accessed for free:

<http://www.sciencemag.org/cgi/content/full/326/5955/962#otherarticles>

This article has been **cited by** 3 articles hosted by HighWire Press; see:

<http://www.sciencemag.org/cgi/content/full/326/5955/962#otherarticles>

This article appears in the following **subject collections**:

Planetary Science

[http://www.sciencemag.org/cgi/collection/planet\\_sci](http://www.sciencemag.org/cgi/collection/planet_sci)

Information about obtaining **reprints** of this article or about obtaining **permission to reproduce this article** in whole or in part can be found at:

<http://www.sciencemag.org/about/permissions.dtl>

erentially where the field is perpendicular to IBEX's radial LOS. A simulation including this effect but using only isotropic distributions showed a weak ENA signal (2). Producing a strong, narrow feature would require the PUIs to remain a ring distribution, in the face of instabilities, long enough for many to neutralize. It is also possible that the ribbon ENAs come from inside the TS, perhaps from shock-accelerated PUIs (26) propagating inward through the region where the solar wind decelerates by  $\sim 20\%$  over  $\sim 10$  AU, just inside the shock (27).

The brightest regions of the ribbon occur well away from the nose and at latitudes where the slow and fast solar winds interact, forming corotating interaction regions. This suggests that the emissions in the ribbon are at least partially related to the solar wind properties as well as to the external environment. Additionally, although the ribbon appears as a continuous feature, it could be a string of more localized, overlapping "knots" of emission. Certainly other ideas need to be examined, and while our data support some earlier

ideas, in other areas a completely new paradigm is needed for understanding the interaction between our heliosphere and the galactic environment.

#### References and Notes

- H. Fahr *et al.*, *Rev. Geophys.* **45**, RG4003 (2007).
- V. V. Izmodenov *et al.*, *Space Sci. Rev.* **146**, 329 (2009).
- M. A. Lee *et al.*, *Space Sci. Rev.* **146**, 275 (2009).
- G. P. Zank *et al.*, *Space Sci. Rev.* **146**, 295 (2009).
- D. J. McComas *et al.*, *Space Sci. Rev.* **146**, 11 (2009).
- S. A. Fuselier *et al.*, *Space Sci. Rev.* **146**, 117 (2009).
- H. O. Funsten *et al.*, *Space Sci. Rev.* **146**, 75 (2009).
- E. Möbius *et al.*, *Science* **326**, 969 (2009); published online 15 October 2009 (10.1126/science.1180971).
- E. C. Stone *et al.*, *Science* **309**, 2017 (2005).
- E. C. Stone *et al.*, *Nature* **454**, 71 (2008).
- S. A. Fuselier *et al.*, *Science* **326**, 962 (2009); published online 15 October 2009 (10.1126/science.1180981).
- H. O. Funsten *et al.*, *Science* **326**, 964 (2009); published online 15 October 2009 (10.1126/science.1180927).
- S. M. Krimigis, D. G. Mitchell, E. C. Roelof, K. C. Hsieh, D. J. McComas, *Science* **326**, 972 (2009); published online 15 October 2009 (10.1126/science.1181079).
- B. E. Wood *et al.*, *Astrophys. J.* **657**, 609 (2007).
- P. Wurz *et al.*, *Astrophys. J.* **683**, 248 (2008).
- R. Lallement *et al.*, *Science* **307**, 1447 (2005).
- M. Opher *et al.*, *Astrophys. J.* **640**, L71 (2006).
- D. J. McComas *et al.*, *Geophys. Res. Lett.* **35**, L18103 (2008).
- H. Washimi *et al.*, *Astrophys. J.* **670**, L139 (2007).
- N. V. Pogorelov *et al.*, *Astrophys. J.* **695**, L31 (2009).
- N. A. Schwadron *et al.*, *Science* **326**, 966 (2009); published online 15 October 2009 (10.1126/science.1180986).
- J. D. Richardson *et al.*, *Geophys. Res. Lett.* **36**, L10102 (2009).
- R. B. Decker *et al.*, *AIP Conf. Proc.* **932**, 197 (2007).
- V. B. Baranov *et al.*, *Astron. Astrophys.* **261**, 341 (1992).
- S. N. Borovikov *et al.*, *Astrophys. J.* **682**, 1404 (2008).
- S. V. Chalov, H. J. Fahr, *Astron. Astrophys.* **311**, 317 (1996).
- J. D. Richardson *et al.*, *Nature* **454**, 63 (2008).
- E. N. Parker, *Astrophys. J.* **134**, 20 (1961).
- We thank all the men and women who made the IBEX mission possible. IBEX was primarily funded by NASA as a part of the Explorers Program (contract NNG05EC85C); foreign investigators were supported by their respective national agencies and institutions.

21 August 2009; accepted 2 October 2009

Published online 15 October 2009;

10.1126/science.1180906

Include this information when citing this paper.

## Width and Variation of the ENA Flux Ribbon Observed by the Interstellar Boundary Explorer

S. A. Fuselier,<sup>1\*</sup> F. Allegrini,<sup>2,3</sup> H. O. Funsten,<sup>4</sup> A. G. Ghielmetti,<sup>1</sup> D. Heitzler,<sup>5</sup> H. Kucharek,<sup>5</sup> O. W. Lennartsson,<sup>1</sup> D. J. McComas,<sup>2,3</sup> E. Möbius,<sup>5</sup> T. E. Moore,<sup>6</sup> S. M. Petrinec,<sup>1</sup> L. A. Saul,<sup>7</sup> J. A. Scheer,<sup>7</sup> N. Schwadron,<sup>8</sup> P. Wurz<sup>7</sup>

The dominant feature in Interstellar Boundary Explorer (IBEX) sky maps of heliospheric energetic neutral atom (ENA) flux is a ribbon of enhanced flux that extends over a broad range of ecliptic latitudes and longitudes. It is narrow ( $\sim 20^\circ$  average width) but long (extending over  $300^\circ$  in the sky) and is observed at energies from 0.2 to 6 kilo-electron volts. We demonstrate that the flux in the ribbon is a factor of 2 to 3 times higher than that of the more diffuse, globally distributed heliospheric ENA flux. The ribbon is most pronounced at  $\sim 1$  kilo-electron volt. The average width of the ribbon is nearly constant, independent of energy. The ribbon is likely the result of an enhancement in the combined solar wind and pickup ion populations in the heliosheath.

The scientific objective of the Interstellar Boundary Explorer (IBEX) is to discover the global interaction between the Sun's solar wind and the interstellar medium (1). This objective is accomplished through the use of two high-sensitivity neutral atom cameras that detect ENAs from 0.01 to 6 keV. Here, the full energy range of the IBEX payload is used to investigate

average characteristics of the ribbon of enhanced hydrogen flux (Fig. 1) detected by IBEX across a large fraction of the sky (2).

The sky map for 0.2-keV hydrogen [see Fig. 1G in (2)] shows evidence of enhanced 0.2-keV hydrogen flux that generally follows the ribbon seen in Fig. 1. In the 0.2-keV sky map, there is also a high-flux region centered approximately on the ecliptic from roughly the nose direction to  $-150^\circ$  longitude. A similar region is evident in a sky map of oxygen (3). These are interstellar oxygen neutrals originating from the nose. The interstellar oxygen is not observed exactly in the nose direction because neutrals are deflected by the Sun's gravity and IBEX measures them in the Earth's reference frame (3). Energetic oxygen neutrals create a hydrogen signature in the IBEX-Lo sensor by knock-off of

negative hydrogen ions from the sensor's neutral-to-negative ion conversion surface (4). Thus, the high-flux region in the 0.2-keV sky map near the nose is not associated with heliospheric hydrogen. Rather, it is a secondary product in the IBEX-Lo sensor from interstellar oxygen. Indeed, sky maps at  $E < 0.2$  keV (3) are dominated by the secondary hydrogen flux produced by both interstellar oxygen and helium in the sensor, and it is difficult to identify a ribbon at energies below 0.2 keV. Thus, the ribbon extends from 0.2 to 6 keV [the upper energy of the 4.3-keV sky map in (2)].

To investigate average properties of the ribbon, we integrated the maps at each energy parallel to the thick black curve in Fig. 1 in  $6^\circ$ -wide bins. These integrals define the average cross section profile of the ribbon (Fig. 2A). The ribbon is centered near  $-3^\circ$  for all energies, except at 0.2 keV. It is not symmetric about  $0^\circ$  because there is structure in the ribbon at higher angular resolution than shown here (2). The ribbon is a flux enhancement above a more diffuse, globally distributed heliospheric ENA flux (2, 5) (the fluxes at  $[-30, -24^\circ]$  and  $[24, 30^\circ]$  define the distributed flux). It is most pronounced at 0.9 keV, where it is a factor of 2.3 times more intense than the distributed flux. At both higher and lower energies, the average intensity of the ribbon decreases so that at 0.2 and 2.7 keV, the ribbon flux is only  $\sim 25\%$  more intense than the distributed flux. The ribbon is centered in the same location up to 6 keV [the highest IBEX energy; see Fig. 1F in (2)].

At 0.2 keV, the influence of the interstellar neutrals is seen from  $12^\circ$  to  $30^\circ$ . In addition, the ribbon appears to be wider and somewhat displaced from the location at all other energies. Below 0.2 keV, it is difficult to identify a ribbon because hydrogen created in the sensor from

<sup>1</sup>Lockheed Martin Advanced Technology Center, Palo Alto, CA 94304, USA. <sup>2</sup>University of Texas at San Antonio, San Antonio, TX 78249, USA. <sup>3</sup>Southwest Research Institute, San Antonio, TX 78228, USA. <sup>4</sup>Los Alamos National Laboratory, Los Alamos, NM 87545, USA. <sup>5</sup>University of New Hampshire, Durham, NH 03824, USA. <sup>6</sup>Goddard Space Flight Center, Greenbelt, MD 20771, USA. <sup>7</sup>University of Bern, Physikalisches Institut, 3012 Bern, Switzerland. <sup>8</sup>Boston University, Boston, MA 02215, USA.

\*To whom correspondence should be addressed. E-mail: stephen.a.fuselier@lmco.com

interstellar neutral helium and oxygen overlaps the ribbon signal (3).

Figure 2A seems to suggest that the width of the ribbon increases at energies both above and below 0.9 keV. However, the real effect is a decrease in the intensity of the ribbon relative to the distributed ENA flux both above and below 0.9 keV. To remove this energy-dependent distributed component, a very shallow parabola was fitted to the distributed components in Fig. 2A (at  $[-30, -24^\circ]$  and  $[24, 30^\circ]$ ), this curve was

subtracted, and the results were renormalized to the flux at  $0^\circ$  (Fig. 2B).

From 0.7 to 2.7 keV, the width of the ribbon is independent of energy, and the full width at half maximum of the ribbon is  $20^\circ$ . At 0.2 keV, the ribbon width is larger and shifted from its location at  $-3^\circ$  (and the presence of a secondary hydrogen signal created from interstellar neutral helium and oxygen in the sensor is still evident at angles  $>12^\circ$ ).

There are statistically significant variations in both the width of the ribbon and its intensity

relative to the distributed flux. For example, the ribbon flux at 1.1 keV varies by about a factor of 2 along its length, and the width varies from about  $15^\circ$  to  $25^\circ$ . Furthermore, there are statistically significant variations in the ribbon profile across the width at angular resolution  $<6^\circ$  (2). These variations are manifested in the asymmetric ribbon location in Fig. 2, A and B.

Heliospheric ENAs are created by charge exchange of solar wind and pickup ions with interstellar neutrals that penetrate the heliopause. The observed ENA flux in any given direction in the sky is the integral of the neutral flux along the line of sight (LOS). Thus, a flux enhancement like the ribbon indicates that there is either a corresponding enhancement in the parent ion flux along the LOS, or a longer LOS for ion charge exchange. The neutral flux is enhanced over a broad energy range and is greatest at 0.9 keV. These two features indicate that the parent ion population of the ribbon is the combined solar wind and pickup ions as they propagate into the heliosheath. Because the enhancement occurs over a broad energy range, ion fluxes of several origins (i.e., decelerated solar wind, pickup ions, and accelerated pickup ions) must be enhanced along the LOS.

Such a narrow ( $20^\circ$  wide) but very long, coherent structure in the sky suggests that magnetic fields play an important role (2). Indeed, the ribbon appears to be oriented in the sky along the curve where the predicted interstellar magnetic field (external to the heliopause) is normal to the radial direction from the Sun (6).

At the solar wind termination shock [assumed to be at 100 astronomical units (AU); 1 AU =  $1.5 \times 10^{10}$  km], the  $20^\circ$  width of the ribbon translates to a spatial width of  $\sim 35$  AU. At the heliopause (assumed to be at 150 AU), the width increases to  $\sim 50$  AU. These widths are small compared to the dimensions of these respective boundaries, but are very large compared to scale lengths like the gyroradius of a 1-keV proton.

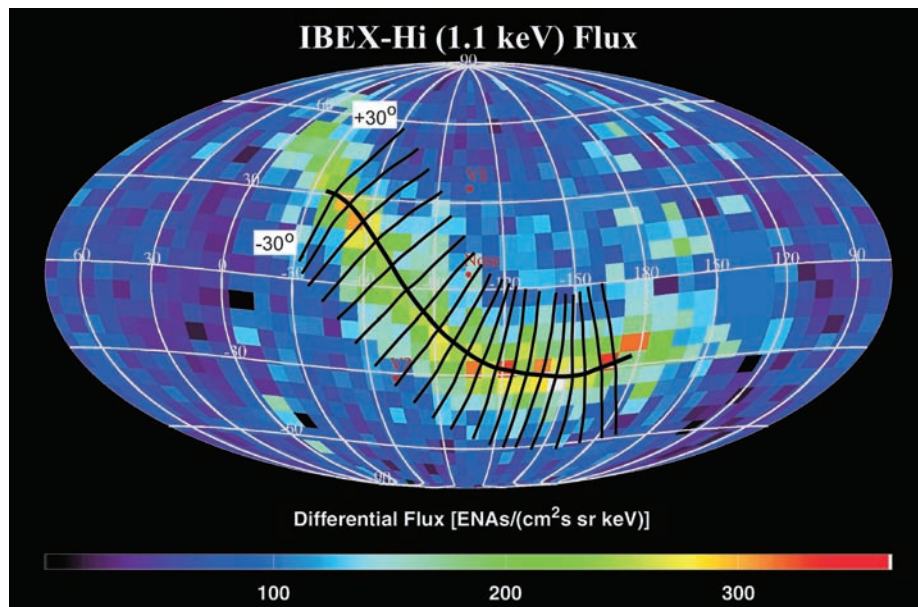
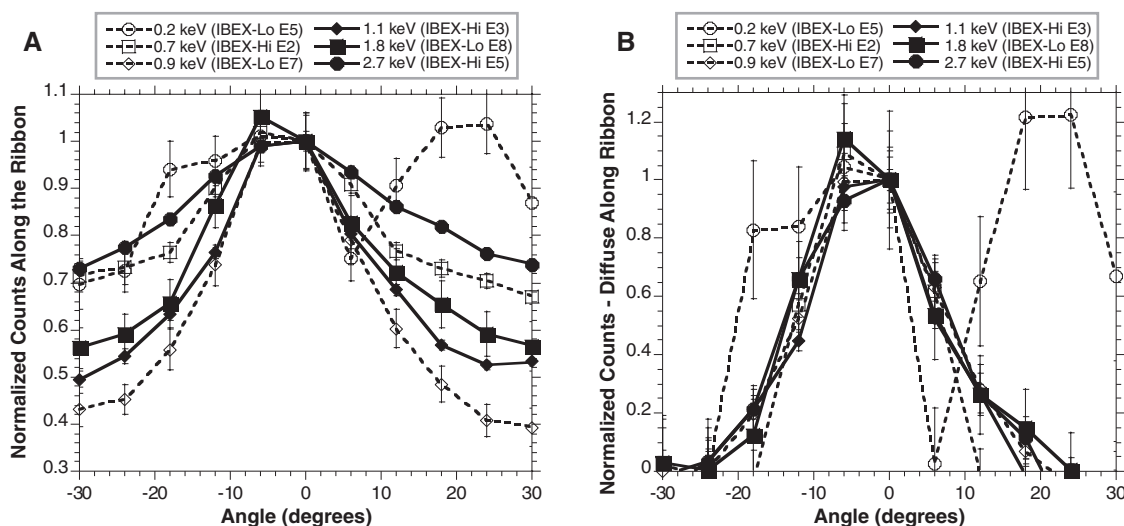


**Fig. 1.** Sky map of 1.1-keV neutral hydrogen flux [in  $\text{cm}^2 \text{ s sr keV}^{-1}$ ] from the IBEX-Hi sensor from the first 6 months of the IBEX mission. This standard IBEX sky map is an oblique Mollweide projection in ecliptic coordinates. The nose direction (the direction of motion of the Sun with respect to the local interstellar medium) is in the center and the tail direction (opposite the nose) is on both the left- and right-hand sides. The map is tilted by  $\sim 5^\circ$  so that the nose direction is exactly in the middle, with north (south) nearly at the top (bottom). The pixel size is  $\sim 6^\circ$ . The dominant feature in this sky map is a ribbon of enhanced ENA flux stretching from  $-30^\circ$  to  $-180^\circ$  ecliptic longitude. The thick, black line traces this ribbon. The short lines show the directions perpendicular to the ribbon out to  $\pm 30^\circ$  and are used to determine the average width of the ribbon.

**Fig. 2.** (A) Average profile of the ribbon for energies from 0.2 to 2.7 keV. These average profiles were obtained by integrating parallel curves that follow the peak flux in the ribbon (Fig. 1) and then normalized by the peak (at  $0^\circ$ ). Dashed lines with open symbols show energies up to 1 keV. Solid lines with filled symbols show energies above 1 keV. Error bars are 1 SD from the mean. The ribbon is most pronounced above the globally distributed heliospheric flux at energies near 1 keV. (B) Average profile of the ribbon for energies above and below 1 keV with the distributed flux from Fig. 2A removed. The width of the ribbon is the same for energies from 0.7 to 2.7 keV.



Identifying the ribbon over a broad energy range has implications for its stability. ENAs with energies of 1 keV take ~1.1 years to propagate from 100 AU to Earth, whereas ENAs with energies of 0.2 keV take ~2.4 years to make the same journey. Thus, the ribbon must exist over at least ~1 year.

#### References and Notes

1. D. J. McComas *et al.*, *Space Sci. Rev.* 10.1007/s11214-009-9499-4 (2009).

2. D. J. McComas *et al.*, *Science* **326**, 959 (2009); published online 15 October 2009 (10.1126/science.1180906).  
 3. E. Möbius *et al.*, *Science* **326**, xxx (2009); published online 15 October 2009 (10.1126/science.1180971).  
 4. S. A. Fuselier *et al.*, *Space Sci. Rev.* 10.1007/s11214-009-9495-8 (2009).  
 5. H. O. Funsten *et al.*, *Science* **326**, 964 (2009); published online 15 October 2009 (10.1126/science.1180927).  
 6. N. A. Schwadron *et al.*, *Science* **326**, 966 (2009); published online 15 October 2009 (10.1126/science.1180986).

7. These results from the IBEX mission are a tribute to the hard work of many scientists and engineers. Work at Lockheed Martin was funded by NASA through sub-contract from Southwest Research Institute.

24 August 2009; accepted 2 October 2009

Published online 15 October 2009;  
 10.1126/science.1180981

Include this information when citing this paper.

# Structures and Spectral Variations of the Outer Heliosphere in IBEX Energetic Neutral Atom Maps

H. O. Funsten,<sup>1\*</sup> F. Allegrini,<sup>2,3</sup> G. B. Crew,<sup>4</sup> R. DeMajistre,<sup>5</sup> P. C. Frisch,<sup>6</sup> S. A. Fuselier,<sup>7</sup> M. Gruntman,<sup>8</sup> P. Janzen,<sup>9</sup> D. J. McComas,<sup>2,3</sup> E. Möbius,<sup>10</sup> B. Randol,<sup>3,2</sup> D. B. Reisenfeld,<sup>9</sup> E. C. Roelof,<sup>5</sup> N. A. Schwadron<sup>11</sup>

The Interstellar Boundary Explorer (IBEX) has obtained all-sky images of energetic neutral atoms emitted from the heliosheath, located between the solar wind termination shock and the local interstellar medium (LISM). These flux maps reveal distinct nonthermal (0.2 to 6 kilo-electron volts) heliosheath proton populations with spectral signatures ordered predominantly by ecliptic latitude. The maps show a globally distributed population of termination-shock-heated protons and a superimposed ribbonlike feature that forms a circular arc in the sky centered on ecliptic coordinate (longitude  $\lambda$ , latitude  $\beta$ ) = (221°, 39°), probably near the direction of the LISM magnetic field. Over the IBEX energy range, the ribbon's nonthermal ion pressure multiplied by its radial thickness is in the range of 70 to 100 picodynes per square centimeter AU (AU, astronomical unit), which is significantly larger than the 30 to 60 picodynes per square centimeter AU of the globally distributed population.

**E**nergetic neutral atoms (ENAs) are formed when energetic ions in the heliosheath, predominantly  $H^+$ , are neutralized by charge exchange with the neutral component of the interstellar gas, predominantly  $H^0$ . Imaging and spectroscopy of these ENAs are used to remotely survey the structure and dynamics of heliosheath plasmas (1, 2). The IBEX-Lo (3) and IBEX-Hi imagers (4) on the Interstellar Boundary Explorer (IBEX) mission (5) measure heliosheath ENAs over the energy range from ~0.2 to 6 keV. The IBEX-Hi and IBEX-Lo all-sky maps show a ribbon (6, 7) that was not anticipated by current models of the structure and dynamics of the interaction region (8). The ribbon is superim-

posed on a globally distributed ENA flux that varies slowly over the sky (6). Here we characterize the underlying plasma structures in the heliosheath by analyzing the spectral index derived from the ENA flux maps (6) both inside and outside the ribbon.

The ENA spectra show two distinct spectral shapes independent of ecliptic longitude  $\lambda$  (Fig. 1, A to C). The blue (north) and red (south) spectra are similar in shape, even though their corresponding intensities vary over a factor of ~2 to 3, with higher intensities in the ribbon. They all exhibit a conspicuous flattening of their slopes for energies >1 keV, which is the characteristic energy range for pickup ions in the fast solar wind that are further heated at the termination shock (9). At each energy passband, the ENA fluxes of all north and south spectra of Fig. 1, A to C (except for the northern tail, which contains the ribbon), are similar, with average fluxes of 192, 79, 30, 17, and 8.7  $cm^{-2} s^{-1} sr^{-1} keV^{-1}$  at energy passbands centered at 0.7, 1.1, 1.7, 2.7, and 4.3 keV, respectively, and standard deviations within 10% of the average flux values at each energy.

In contrast to the high-latitude spectra, the smooth low-latitude (green) spectra can be approximated as a power law spectrum with a single spectral index  $\kappa$  (8). This applies even in the ribbon, which exhibits a larger overall in-

tensity but a similar single slope as compared to nonribbon spectra (Fig. 2, A and C). The value of  $\kappa$  at low latitudes shows a weak trend with longitude (Fig. 1D), with fits of the data over the nine energy channels yielding  $\kappa = 1.5$  for the nose and  $\kappa = 2.1$  for the tail. The nose and tail spectral shapes are also slightly but consistently different, possibly resulting from longer line-of-sight (LOS) integrations of low-energy ions toward the tail. Another exception is the spectrum in the direction of Voyager 1 (6), which is more characteristic of high-latitude spectra.

The spectral index  $\kappa$  at higher energies is predominantly ordered by ecliptic latitude  $\beta$  (Fig. 2, A and B). The spectral indexes within the ribbon nearly overlap with and show the same strong latitude dependence as the globally distributed flux outside the ribbon. For the globally distributed flux that does not include the ribbon, the average spectral index at low latitudes ( $-30^\circ \leq \beta \leq 30^\circ$ ) is  $\kappa = 1.95 \pm 0.09$  at 1.7 keV and  $\kappa = 1.91 \pm 0.07$  at 2.7 keV, and at high latitudes ( $\beta \leq -54^\circ$ ,  $\beta \geq 54^\circ$ ) is  $\kappa = 1.49 \pm 0.05$  and  $\kappa = 1.36 \pm 0.08$ , respectively, revealing a distinctly different higher-energy ion population at high latitude.

These observations show that the global characteristics of nonthermal heliosheath ions are ordered predominantly by ecliptic latitude, regardless of whether they reside inside or outside of the ribbon. Because ecliptic latitude is almost indistinguishable from heliographic latitude, this spectral signature is probably imposed by the latitude dependence of the solar wind, whose transition from slow (equatorial) to fast (polar) solar wind in the outer heliosphere occurs at mid-latitudes throughout the present minimum phase of the solar cycle (10). It also suggests that the intensity features of the ribbon are not produced by local heliosheath acceleration processes that would presumably impose a different spectral signature associated only with these higher fluxes. If the solar wind orders the spectral characteristics of heliosheath plasma, we expect temporal variation of the globally distributed flux, and possibly structures such as the ribbon, caused by the changing solar wind pattern throughout the 11-year (and possibly 22-year) solar cycle.

We divided the ribbon into three regions based on differences in spectral signature (Fig. 2, C and D). The spectra of regions 1 and 3 are consistent with the spectral signatures of low- and high-latitude regions, respectively (Fig. 1, A

<sup>1</sup>Los Alamos National Laboratory, Los Alamos, NM 87545, USA.

<sup>2</sup>Southwest Research Institute, San Antonio, TX 78228, USA.

<sup>3</sup>University of Texas at San Antonio, San Antonio, TX 78249, USA.

<sup>4</sup>Massachusetts Institute of Technology, Cambridge, MA 02139, USA.

<sup>5</sup>Applied Physics Laboratory, Johns Hopkins University, Laurel, MD 20723, USA.

<sup>6</sup>University of Chicago, Chicago, IL 60637, USA.

<sup>7</sup>Lockheed Martin Advanced Technology Center, Palo Alto, CA 94304, USA.

<sup>8</sup>University of Southern California, Los Angeles, CA 90089-1192, USA.

<sup>9</sup>University of Montana, Missoula, MT 59812, USA.

<sup>10</sup>University of New Hampshire, Morse Hall, Durham, NH 03824, USA.

<sup>11</sup>Boston University, Boston, MA, 02215, USA.

\*To whom correspondence should be addressed. E-mail: hfunsten@lanl.gov